Proceedings of the 2006 IASME/WSEAS International Conference on Continuum Mechanics, Chalkida, Greece, May 11-13, 2006 (pp91-96)

A comparative numerical study of a non-Newtonian blood flow model

ABDELMONIM ARTOLI
Inst. Superior Técnico
Dept. Matemática and CEMAT
Av. Rovisco Pais, 1049 LISBOA
PORTUGAL

JOÃO JANELA
Inst. Sup. Economia e Gestão
Dept. Matemática and CEMAT/IST
Rua do Quelhas, 6, 1200 LISBOA
PORTUGAL

ADÉLIA SEQUEIRA
Inst. Superior Técnico
Dept. Matemática and CEMAT
Av. Rovisco Pais, 1049 LISBOA
PORTUGAL

Abstract: Pulsatile non-Newtonian blood flow in an idealized vessel is numerically investigated. The Carreau-Yasuda model is used to account for the shear-thinning viscosity of blood. For validation purposes, we have used two numerical methods: a mesoscopic lattice-Boltzmann equation and a standard finite element solver. Good agreement for the velocity and the shear stress has been obtained from the two approximate solutions for the assigned laminar flow conditions. The coupling of the two methods to deal with more complex flows in realistic geometries is under development.

Key–Words: unsteady flow, shear-thinning fluid, Carreau-Yasuda model, mesoscopic hemodynamics, finite element method.

1 Introduction

Cardiovascular diseases represent a major cause of mortality in the world (see e.g. [7]). It is now commonly accepted that hemodynamics plays an important role in the localization and development of arterial diseases and can have useful applications in medical research, surgical planning and therapy to restore blood flow in pathological organs and tissues. For instance, in the case of atherosclerosis numerous studies report that hemodynamic factors such as low and oscillatory shear stress, temporal and spatial variation of wall tension play crucial roles. These findings allow to identify risk factors in spots of low shear stress regions, high pressure distributions along the vessels or high particle residence times in the cardiovascular system. Currently, experimental measurements of blood flow velocity and pressure drop in the vasculature involve both invasive and non-invasive techniques such as intra-vascular ultrasound probes [10], electromagnetic flow probes [14] or magnetic resonance imaging [15]. The corresponding collected data are accurate enough for quantification of some aspects of the arterial diseases but are very sensitive to disturbing factors. This results in difficult interpretations in most relevant cases. The role of computational fluid dynamics (CFD) in quantifying local hemodynamics for each specific patient and in designing enhanced devices is gaining more ground and may be included as a routine clinical investigation in the future.

In a simplistic approach, blood can be modelled as a suspension of erythrocytes (red blood cells), the most numerous of the formed elements (about 98%) in an aqueous polymer solution, the plasma. This approach is incomplete in the sense that it ignores many other components of blood (leukocytes, platelets, suspended salts, proteins and other matter), but is reasonable since red blood cells (RBCs) represent about 45% of the volume of normal human blood and are by two orders of magnitude more numerous than all other suspended particles. The RBCs tend to aggregate at low shear rates forming complex structures named *rouleaux* and these aggregates break at higher shear rates. Ignoring the viscoelastic effects due to dissipation and storage of elastic energy, and considering only the shear-dependent blood viscosity caused by the formation and destruction of *rouleaux*, an empirical model for describing blood flow, obtained by fitting experimental data in one dimensional flows is the shear-thinning Carreau–Yasuda model [4] given by

$$\eta(\dot{\gamma}) = \eta_\infty + (\eta_0 - \eta_\infty)\left[1 + (\lambda\dot{\gamma})^a\right]^{\frac{n-1}{a}} \qquad (1)$$

Here η_0 and η_∞ are the asymptotic viscosities at low and high shear rates, λ is a characteristic ~~rel~~axation time and a, n are parameters used to fit experimental data. When $a = 0$ or $n = 1$ the fluid behaves as Newtonian. When $a \neq 0$ and $n < 1$ the fluid is shear-thinning (the viscosity decreases with shear rate). Here we consider the following parameter val-

ues for blood flow $\eta_0 = 0.022$ Pa s, $\eta_\infty = 0.0022$ Pa s, $\lambda = 0.11$ s, $a = 0.644$ and $n = 0.392$ (see e.g. [5]).

2 Governing equations and numerical methods

2.1 Problem definition

We consider pulsatile flow of an incompressible non-Newtonian fluid in a three-dimensional tube, possibly curved and irregular. Even though our numerical simulations will be conducted in straight tubes with constant cross section, this is not relevant to the usage of the numerical solvers, which are prepared to accept realistic geometries such as the one shown in figure 2.1, resulting from medical imaging data.

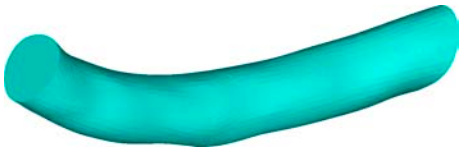

Figure 1: Geometric reconstruction of a segment of a real artery obtained by magnetic resonance imaging (MRI).

To fix notation, consider an open regular set $\Omega_t \subset \mathbb{R}^3$, representing the interior of a vessel at time t and denote by $\Gamma_t^w, \Gamma_t^{in}$ and Γ_t^{out} the vessel lateral wall, inlet boundary and outlet boundary, respectively. Denoting by $\boldsymbol{u}$ and p the fluid's velocity and pressure and by $\boldsymbol{\sigma}$ the Cauchy stress tensor, the governing equations can be derived from the conservation of linear momentum

$$\rho\frac{\partial \boldsymbol{u}}{\partial t} + \rho(\boldsymbol{u}\cdot\nabla\boldsymbol{u}) = \nabla\cdot\boldsymbol{\sigma} + \boldsymbol{f} \qquad \text{in } \Omega_t \qquad (2)$$

where ρ is the constant density and $\mathbf{f}$ are the external body forces per unit volume (e.g. gravity).
The incompressibility condition reads

$$\nabla\cdot\boldsymbol{u} = 0 \qquad \text{in } \Omega_t \qquad (3)$$

Equations (2) and (3) are coupled with a constitutive equation for the stress tensor, $\boldsymbol{\sigma}$,

$$\boldsymbol{\sigma} = -p\mathbf{I} + \eta(\dot\gamma)(\nabla\boldsymbol{u} + (\nabla\boldsymbol{u})^T) \qquad (4)$$

where $\boldsymbol{\tau} = \eta(\dot\gamma)(\nabla\boldsymbol{u}+(\nabla\boldsymbol{u})^T)$ is the extra stress tensor and the functional relation between shear rate and viscosity $\eta(\dot\gamma)$ is given by the Carreau–Yasuda model (1). Incompressible fluids of this type for which the extra stress tensor is related to the velocity gradient through (4) belong to a class of inelastic non-Newtonian fluids called generalized Newtonian fluids.

The system of equations (2)-(3) must be closed with proper initial and boundary conditions. This usually reduces to prescribing either the velocity field or tangential and normal components of the stress vector in Γ^{in} and Γ^{out}. We prefer to consider the flow as being driven by a pressure drop, but this must be done in a careful way since only for fully developed outflow velocities a prescribed normal component of the stress vector (together with zero tangential velocity) corresponds to a prescribed pressure.
In the sequel we will further assume that the tube is rigid and so the domain Ω_t does not depend on time. For this reason the time subscript in the spatial domain and boundaries will be dropped on the notations.

2.2 Weak formulation and finite element approach

The finite element approach requires the differential problem to be written in a variational form. Let us define two Hilbert spaces V and Q. The weak or variational formulation of our problem is obtained by multiplying the governing equations by test functions $\boldsymbol{v} \in V$ and $q \in Q$ and integrating by parts. The use of test functions can be seen as describing indirectly the solution by its effect on them. If we prescribe as boundary condition the normal stress vector $\mathbf{s} = \boldsymbol{\sigma}\cdot\mathbf{n}$ in $\Gamma = \Gamma^{in} \cup \Gamma^{out}$, together with no-slip boundary conditions in $\Omega - \Gamma$, our problem consists in finding $\boldsymbol{u} \in V$ and $p \in Q$ such that,

$$\int_\Omega \rho\frac{D\boldsymbol{u}}{Dt}\cdot\boldsymbol{v} + \int_\Omega \boldsymbol{\tau} : \nabla\boldsymbol{v} - \int_\Omega p\nabla\cdot\boldsymbol{v} =$$

$$\int_\Omega \boldsymbol{f}\cdot\boldsymbol{v} + \int_\Gamma \mathbf{s}\cdot\boldsymbol{v}, \qquad \forall\boldsymbol{v}\in V$$

and

$$\int_\Omega q\nabla\cdot\boldsymbol{u} = 0, \qquad \forall q \in Q.$$

The discretization in time is done by a suitable second order trapezoidal rule/back-differentiation formula and the discretization in space uses a standard Petrov–Galerkin method (see e.g. [12]). To apply the Galerkin method we discretize the spatial domain Ω and introduce two families $\{V_h \mid h > 0\}$ and $\{Q_h \mid h > 0\}$ of finite element subspaces of V and Q, respectively, satisfying a compatibility condition, the so-called *discrete inf-sup* or *LBB condition*. The solution is approximated by piecewise polynomial functions on each element of the discretized domain. These polynomials must be chosen in such a way that the discrete inf-sup condition is fulfilled, otherwise the *locking* phenomenon for the velocity

field or *spurious pressure modes* can occur. For instance equal order interpolation for both the velocity and pressure unknowns does not verify the inf-sup condition. The most common discretization technique is $P2-P1$ (piecewise quadratic elements for the velocity and linear elements for the pressure) or $P1\,iso\,P2-P1$ where the velocity is linear over each of the four sub-elements obtained by joining the midpoints of the edges of each pressure element. Since the spaces of piecewise polynomials are of finite dimension, the substitution of the functions in the weak formulation by their expansions in the basis of the discrete spaces leeds, after the numerical evaluation of the integrals, to a nonlinear system of finite dimension. The resulting system is then linearized, at each time step, using an iterative Newton-like method. Error bounds can be derived for the numerical solution of this problem, based on the size of the mesh used to discretize the domain and on the type of finite elements (regularity across elements and interpolation order).

2.3 Lattice–Boltzman method for shear-thinning fluids

Simulations of complex fluids such as blood are characterized by the existence of time-scale phenomena. Typical parameters may range from mesoscale to macroscale. This makes it difficult for a single numerical solver to capture the complete behaviour and deal with the whole complexity of the fluid and the containing vessel. Most commercial numerical solvers allow simulations of shear-thinning fluids through defining a shear-dependent viscosity which is a function of the shear-rate. However, the interdependency of the shear rate computed from the velocity gradients and the viscosity complicates the regime. The finite element approach described in the previous section is quite adequate and accurate for simulation of non-Newtonian fluids and for fluid-structure interactions. However, due to the lack of analytical solutions for the Carreau-Yassuda model and difficulties in obtaining accurate experimental results, comparison with other numerical methods becomes mandatory. This is the goal of using the lattice–Boltzmann as an independent mesoscopic solver for shear-thinning fluids. Although the method is relatively new (about two decades), it has been successfully used in simulations of non-Newtonian fluids such as viscoelastic [11], [9], citeoldroyd, power-law [13], Cross [6] and Carreau-Yasuda fluids [2]. Due to its inherent parallelism and straightforward implementation and also to its capability to deal with suspension fluids, we have chosen an adaptation of the lattice–Boltzmann method for shear–thinning fluids recently proposed by Artoli and Sequeira [2].

The lattice–Boltzmann equation is a special finite difference discretization of the simplified Boltzmann equation (see e.g. [3]) which describes transport phenomena at the mesoscale level. The fluid motion is modelled by the transport of simple fictitious particles on the nodes of a Cartesian grid. Simulations with this method involve two simple steps: streaming to the neighbouring nodes and colliding with local node populations represented by the probability f_i of a particle moving with a velocity $\mathbf{e}_i$ per unit time step δt. Populations are relaxed towards their equilibrium states during a collision process. The equilibrium distribution function is a low Mach number approximation to the Maxwellian distribution. The lattice–Boltzmann equation

$$f_i(\mathbf{x}+\mathbf{e}_i\delta t, \mathbf{e}_i, t+\delta t) - f_i(\mathbf{x}, \mathbf{e}_i, t) = \Lambda$$

where $\Lambda = -\frac{1}{\tau}[f_i(\mathbf{x}, \mathbf{e}_i, t) - f_i^{(0)}(\mathbf{x}, \mathbf{e}_i, t)]$, can be obtained by discretizing the evolution equation of the distribution functions in the velocity space using a finite set of velocities $\mathbf{e}_i$. In this equation, τ is the dimensionless relaxation time which links the microscopic evolution and the macroscopic average thermodynamic behaviour of the fluid. By Taylor expansion of the lattice–Boltzmann equation and application of the multiscale Chapman-Enskog technique [3], the Navier-Stokes equations and the momentum flux tensor up to second order in the Knudsen number are obtained. The hydrodynamic density, ρ, and the macroscopic velocity, $\mathbf{u}$, are determined in terms of the particle distribution functions from the laws of conservation of mass and momentum. The pressure is given by $p = \rho c_s^2$ and the kinematic viscosity is $\nu = c_s^2\delta t(\tau - \frac{1}{2})$, where c_s is the lattice speed of sound. The momentum flux is directly computed from the non-equilibrium part of the distribution functions and the strain rate tensor is

$$S_{\alpha\beta} = -\frac{1}{2C\delta_t\tau_c\rho}\sum_i f_i^{(1)}\mathbf{e}_{i\alpha}\mathbf{e}_{i\beta} \qquad (5)$$

The stress tensor is given by

$$\sigma_{\alpha\beta} = -\rho c_s^2\delta_{\alpha\beta} - \left(1-\frac{1}{2\tau_c}\right)\sum_{i=0} f_i^{(1)} e_{i\alpha}e_{i\beta}. \qquad (6)$$

In constitutive equations of shear-thinning generalized Newtonian fluids the viscosity depends on the magnitude or the second invariant of the strain rate tensor which can be computed from the double inner product of $S_{\alpha\beta}$ by itself

$$|S| \equiv \dot{\gamma} = \sqrt{2S_{\alpha\beta} : S_{\alpha\beta}}. \qquad (7)$$

This is locally computed during collision from the simple relation

$$\dot{\gamma} = \dot{\gamma_c}\sqrt{0.5(S_{xx}^2 + S_{yy}^2 + S_{zz}^2) + (S_{xy}^2 + S_{xz}^2 + S_{yz}^2)} \quad (8)$$

where $\dot{\gamma_c} = \frac{3}{2\rho\tau_c}$ can be used as a characteristic shear rate. In this study we propose that $\tau_c = 1$ to benefit from the simplicity and the accuracy of the scheme at $\tau = 1$. The Carreau-Yasuda viscosity behaviour of blood can be modelled in terms of the dimensionless relaxation times (τ and τ_c)

$$\tau = \tau_\infty + (\tau_0 - \tau_\infty)(1 + (\lambda\dot{\gamma})^a)^b \quad (9)$$

where τ_0 and τ_∞ correspond to η_0 and η_∞, respectively.

3 Numerical simulations

The numerical simulations were carried out in a tube with 2 cm diameter and 4 cm length. This length is large enough to obtain fully developed flows. The flow is driven by a pressure sine wave of type $A \sin \omega t$, where A is the length of the tube. No-slip conditions are applied in the tube lateral wall. The parameters used for the Carreau-Yasuda model are those mentioned above in the introduction (see e. g. [5]).

The convergence criterium was set by comparing corresponding values of the velocity field in successive periods and fixing a tolerance of 1 %.

The results obtained for the velocity and shear stress were compared in a circular cross-section of the tube. Figures 2 and 3 show the velocity profiles obtained by the lattice-Boltzman method (dots) and by the finite element method (lines) in the beginning and at the end of a time period. The agreement is excellent, however the LB profile is more flattened and has higher values in the $[r/4, r/2]$ region of the tube. This may be attributed to an observed small phase lag that is more evident in Figure 4, which depicts the evolution in time of the centerline velocity. The phase lag is clearly observed at the peaks in two successive periods. The lag between velocity and pressure is approximately $\pi/2$, which is in qualitative agreement with the results reported in literature (see [17, 2]).

Concerning the shear stress, despite of the large difference calculation procedures in both methods, excellent agreement has also been noticed, as shown in Figure 5, where the shear stress at the beginning of a period is represented for both LB and FEM. Similar agreement is observed throughout the complete period (data not shown). Again there is a discrepancy (maximum 10 %) between the results of the two methods, especially in the region $[r/4, r/2]$.

Comparative studies of wall shear stress (WSS) were also conducted due to its role in hemodynamics. Figure 6 shows time evolution of WSS over the last two simulated periods. The phase lag appears again, even more prominently. This results in a slight discrepancy of the reported times at which low, oscillatory or high shear stress occurs.

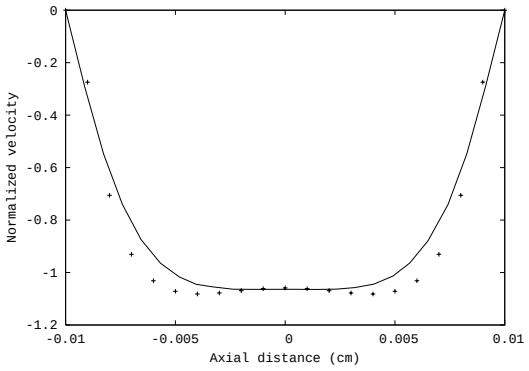

Figure 2: Velocity profile with LB (dots) and FEM (line) at $t = 0$.

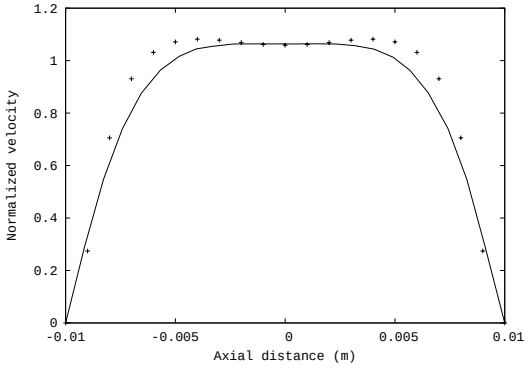

Figure 3: Velocity profile with LB (dots) and FEM (line) at $t = \pi$.

4 Discussion

The non-Newtonian shear-thinning Carreau-Yasuda viscosity law to model blood flow in a straight vessel has been implemented using two independent numerical methods: a finite element Navier-Stokes solver where the shear stress is obtained from the velocity gradients and a lattice–Boltzmann algorithm that solves the mesoscopic Boltzmann equation algorithm and computes the shear stress from the non-equilibrium properties of an evolving fluid. We have shown that the results obtained with both methods are in good agreement, for the non-Newtonian time dependent velocity field and the shear stress, through-

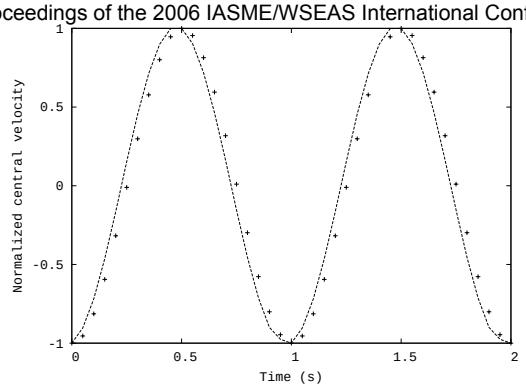

Figure 4: Evolution of the centerline velocity in two successive periods with LB (dots) and FEM (line).

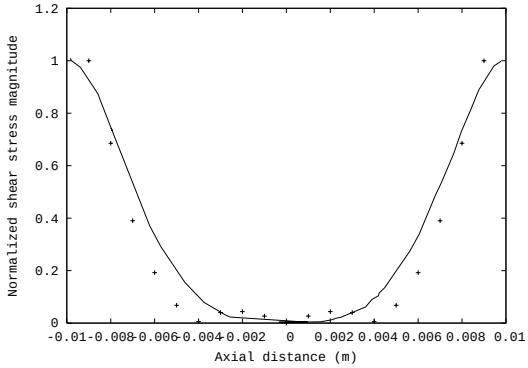

Figure 5: Shear stress magnitude with LB (dots) and FEM (line) at $t = 0$.

out the simulated time period in which the flow is driven by a sine wave. However, a phase lag between the two methods is observed. The lattice–Boltzmann is lagging the finite element method with a small phase. This may be attributed to the difference in time at which measurements are recorded. The lattice–Boltzmann method is known to be more accurate at half time steps ([1]) in two dimensions, but this time shift is negligible in three dimensions. The finite element method consumes considerable computational resources to converge to the right phase. It is not yet clear which one is the most accurate method. This is a subject of ongoing research. A comparison between the results obtained with the shear-thinning and the Newtonian models has reported higher values for the shear stress and oscillations closer to the wall for the shear-thinning fluids, even in large arteries. Therefore, non-Newtonian simulations should be considered if accurate shear stress values are needed. Presently we are interested in using the two numerical techniques in the simulation of this non-Newtonian blood flow model in segments of the carotid artery and of the circle of Willis. The comparison of the two numerical methods in terms of efficiency and computational times is a subject for a future publication as it is not relevant for the validation of results.

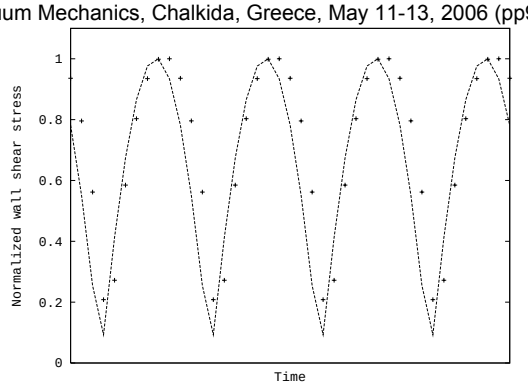

Figure 6: Evolution of the WSS in two successive periods with LB (dots) and FEM (line).

Acknowledgements

This work has been partially supported by the grant SFRH/BPD/20823/2004 of Fundação para a Ciência e a Tecnologia (A. Artoli), by the Center for Mathematics and its Applications - CEMAT through FCTs funding program and by the projects POCTI/MAT/41898/2001 and HPRN-CT-2002-00270 (Research Training Network 'HaeMOdel' of the European Union).

References:

[1] A.M. Artoli, A.G. Hoekstra and P.M.A. Sloot, Accuracy of 2D Pulsatile Flow in the Lattice-Boltzmann BGK Method, *Lecture Notes in Computer Science*, 2002, pp 361–370.

[2] A. M. Artoli and A. Sequeira, Mesoscopic simulations of unsteady shear-thinning flows, *Lecture Notes in Computer Science*, 2006. To appear.

[3] R. Benzi, S. Succi, M. Vergassola, The Lattice Boltzmann Equation - Theory and Applications. Physics Reports, 222, 1992, pp. 145–197.

[4] R.B. Bird, R.C. Armstrong and O. Hassager, *Dynamics of Polymer Liquids Vol. 1*, 1987, Wiley, New York.

[5] F.J.H. Gijsen, E. Allanic, F.N. van de Vosse and J.D. Janssen, The influence of the non-Newtonian properties of blood on the flow in large arteries: steady flow in a carotid bifurcation model, *Journal of Biomechanics*, 32, 1999, 601–608.

[6] D. Kehrwald, Lattice Boltzmann simulation of shear-thinning fluids, *Journal of Statistical Physics*, 121 (1-2), 2005, pp. 223-237.

[7] C.J.L. Murray and D.A. Lopez, *The Global Burden of Disease*, The Harvard School of Public Health and World Health Organization and World Bank, 1996.

[8] J. Onishi, Y. Chen and H. Ohashi, A Lattice Boltzmann model for polymeric liquids, *Progress in Computational Fluid dynamics*, 5 (1–2), 2005, pp. 75–84.

[9] Y.C. Onishy and H. Ohashi, Dynamic simulation of multi-component viscoelastic fluids using the lattice– Boltzmann method, *Physica A*, 362, 2006, pp. 84–92.

[10] M. J. Perko, Duplex Ultrasound for Assessment of Superior Mesenteric Artery Blood Flow, *European Journal of Vascular and Endovascular Surgery*, 21, 2001, pp. 106–117.

[11] Y.H. Qian and Y.F.J. Deng, A lattice BGK model for viscoelastic media, *Physical Review Letters*, 79, 1997, pp. 2742–2745.

[12] A. Quarteroni and A. Valli, *Numerical Approximation of Partial Differential Equations*, Springer Series in Computational Mathematics, Springer-Verlag, Berlin, Heidelberg, 1994.

[13] S.P. Sullivan, L.F. Gladden and M.L. Johns, Simulation of power-law fluid flow through porous media using lattice–Boltzmann techniques, *Journal of Non-Newtonian Fluid Mechanics*, 133, 2006, pp. 91–98.

[14] R. Tabrizchi and M. K. Pugsley, Methods of blood flow measurement in the arterial circulatory system, *Journal of Pharmacological and Toxicological Methods*, 44, 2000, pp. 75–384.

[15] R. Unterhinninghofen, J. Albers, W. Hosch, C. Vahl and R. Dillmann,Flow quantification from time-resolved MRI vector fields, *International Congress Series*, 1281, 2005, pp. 126–130

[16] F.N. Van de Vosse et al., Finite element based computational methods for cardiovascular fluid–structure interaction, *Journal of Engineering Mathematics* 47, 2003, pp. 335–368.

[17] M. Zamir, *The Physics of Pulsatile Flow*, Biological Physics series, Springer–Verlag, New York, 2000.